EUROPEAN ORGANIZATION FOR NUCLEAR RESEARCH

CERN-EP/89-78
28 June 1989

THRESHOLD MEASUREMENT OF THE REACTION $\bar{p}p \rightarrow \bar{\Lambda}\Lambda$ AT LEAR

P. D. Barnes[1], R. Besold[3,a], P. Birien[4], B. E. Bonner[7,b], W. H. Breunlich[9], G. Diebold[1], W. Dutty[4], R. A. Eisenstein[5], G. Ericsson[8], W. Eyrich[3], R. v. Frankenberg[3,c], G. Franklin[1], J. Franz[4], N. Hamann[4], D. Hertzog[5], A. Hofmann[3], T. Johansson[8], K. Kilian[2,c], C. Maher[1], W. Oelert[6], S. Ohlsson[8], H. W. Ortner[3], P. Pawlek[9], B. Quinn[1], E. Rössle[4], H. Schledermann[4], H. Schmitt[4], J. Seydoux[1], and P. Woldt[3]

This paper is dedicated to the memory of our recently deceased friend and colleague, Alfred Hofmann.

1) Carnegie Mellon University, Pittsburgh PA, USA
2) CERN, Geneva, Switzerland
3) University of Erlangen-Nürnberg, Erlangen, FRG
4) University of Freiburg, Freiburg, FRG
5) University of Illinois, Urbana IL, USA
6) Institut für Kernphysik der KFA, Jülich, FRG
7) Los Alamos National Laboratory, Los Alamos NM, USA
8) University of Uppsala, Uppsala, Sweden
9) Institut für Mittelenergiephysik der ÖAW, Vienna, Austria

ABSTRACT

The excitation function of the reaction $\bar{p}p \rightarrow \bar{\Lambda}\Lambda$ in the threshold region has been measured at LEAR. Sixteen measurements of the total cross section, in the energy range between 0.85 MeV below threshold and 4.05 MeV above, are presented. The shapes of the measured differential cross sections indicate a remarkably strong p-wave contribution even down to the reaction threshold. We also report here the measurement of significant polarizations in the threshold region; these are compared with previous higher-energy data.

(Submitted to Physics Letters B)

Present addresses:
a) Siemens AG, Nürnberg, FRG
b) Rice University, Houston, TX, USA
c) Institut für Kernphysik der KFA Jülich, Jülich, FRG

1. INTRODUCTION

The exclusive production of hyperon-antihyperon pairs in $\bar{p}p$ collisions is a particularly attractive channel for investigating $\bar{N}N$ reaction mechanisms. The strangeness produced in the final state offers an opportunity to extract information on individual quarks and their interactions. The production of an $\bar{s}s$ quark pair typically involves large momentum transfers even close to the reaction threshold and is therefore sensitive to the short-range effects of the interaction. Measurement of spin observables in this kinematic region provides additional information on the reaction dynamics. Moreover, measurements near the reaction threshold provide the advantage of limiting the number of relevant partial waves, making the interpretation of the data less complicated.

Modern theoretical descriptions of the reaction $\bar{p}p \rightarrow \bar{\Lambda}\Lambda$ are of two general types. One may invoke a "conventional" t-channel meson-exchange picture in which, because strangeness production is required to create the hyperon-antihyperon final state, a potential derived from kaon exchange is used for calculations [1-4]. Or, at the quark level, one may adopt an s-channel "pseudo gluon exchange" picture in which odd numbers of gluons are represented by a 1^- exchange (the $^3S_1$ model [3,5-8]), while even numbers of exchanged gluons are represented by a 0^+ exchange (e.g. the vacuum pair ($^3P_0$) creation model [5-7]). Both meson- and gluon-exchange models are available to compare with data.

Experiment PS185 at the LEAR facility at CERN was initiated in order to measure very precisely the production of hyperons close to their reaction thresholds. Our first measurements [9] covered the reaction $\bar{p}p \rightarrow \bar{\Lambda}\Lambda$ at incident antiproton momenta of 1476.5 MeV/c and 1507.5 MeV/c, which correspond to energies, ε, above threshold ($\varepsilon = \sqrt{s} - 2m_\Lambda$) of 14.6 MeV and 25.5 MeV, respectively. At these incident momenta the results showed clear evidence of strong contributions from partial waves of angular momentum $l > 0$.

In this paper we report on a threshold-region energy scan of the reaction $\bar{p}p \rightarrow \bar{\Lambda}\Lambda$. In these measurements we examine the ε region from 0.85 MeV below threshold to 4.05 MeV above it. A total of 7.05×10^{10} antiprotons were incident on target, with 1.23×10^7 neutral events recorded; of those, 1442 $\bar{\Lambda}\Lambda$ events have been obtained and analyzed. Differential and total cross sections, as well as polarization data, have been obtained and are presented below.

2. EXPERIMENT

The detector [9] consists of four basic elements: an active-trigger target, sets of multiwire proportional- and drift- chambers for charged track reconstruction, a scintillator

hodoscope for fast charged particle triggering, and a set of drift chambers (placed in a solenoidal magnetic field) that is used as a baryon number identifier for each vertex.

The active-trigger target is used to indicate both the incidence of an antiproton ("beam particle") and a subsequent neutral final state ("neutral trigger"). The desired Λ and $\bar{\Lambda}$ hyperons decay most often within the chamber stack, 41% of the time producing four charged reaction products; the overall event is the process $\bar{p}p \rightarrow \bar{\Lambda}\Lambda \rightarrow \bar{p}\pi^+ p\pi^-$. A signal from the downstream scintillator hodoscope is used to indicate the presence of two or more charged particles in the final state. This fast signal, together with the "neutral trigger" and "beam particle" signals, completes a full "charged-neutral-charged" event trigger.

The components of the track-imaging detector are a stack of 10 multiwire proportional chamber planes followed by a stack of 13 horizontally- and vertically-oriented drift chambers. The stacks are rotated by 45° with respect to each other in order to resolve track ambiguities. Three drift chamber planes inside a 0.1 T solenoid identify hyperon/anti-hyperon by the left/right bending of the charged hadrons from the hyperon decays. More details about the detector can be found in ref. [9].

The major change in the apparatus between the present measurement and the earlier one [9] is the use of a five-cell modular target (Fig. 1). In front of this target there are the two beam-defining scintillators, S1A and S1B; these provide the antiproton tag and give a "start" signal (t = 0) for all subsequent readout processes. The time resolution of these counters is 0.3 ns. Each of the following five target cells consists of a 2.5 mm thick cylinder of material with diameter 2.5 mm. Four of the cells (T2-T5) are made of polyethylene (CH_2) and serve as proton targets, while the first target cell (T1) consists of pure carbon and is used to monitor the carbon background contribution. Each target is surrounded radially by a 1.25 mm thick veto scintillation barrel (S2), and at the front and rear by two counters labelled S3, each with a thickness of 0.2 mm. S2 is used for suppressing background reactions involving charged particles, while the S3 counters provide a clean antiproton tag (or veto) before (or after) each consecutive cell. The charged-trigger rejection inefficiency for each cell was smaller than 10^{-5}. The benefit of the modular target structure is that it allows a step-wise degradation of the incident antiproton beam momentum in fine bins of 0.8 MeV/c, corresponding to the mean momentum loss in each cell. In addition, two polyethylene degraders of 5 mm and 11 mm thickness were used for larger momentum steps of 1.4 MeV/c and 3.1 MeV/c, respectively. The ability to vary the incident momentum in this way was essential to the success of our measurement.

3. DATA ANALYSIS

In our analysis the existence of two neutral decay vertices in the track-imaging part of the detector is the signature for the reaction $\bar{p}p \rightarrow \bar{\Lambda}\Lambda \rightarrow \bar{p}\pi^+ p\pi^-$. To reconstruct these vertices, and to separate good event candidates from possible background reactions, an event selection program has been developed. The basic principles include: fitting three-dimensional tracks to chamber hits; using those tracks in a vertex candidate search; and finally, performing a full kinematic fitting of pairs of matched vertices assuming that the event type is in fact $\bar{p}p \rightarrow \bar{\Lambda}\Lambda \rightarrow \bar{p}\pi^+ p\pi^-$. A good $\bar{\Lambda}\Lambda$ event was defined as one for which the reduced χ^2 fell below 5.

The reconstruction of $\bar{p}p \rightarrow \bar{\Lambda}\Lambda \rightarrow \bar{p}\pi^+ p\pi^-$ events near the production threshold is extremely sensitive to the energy of the incident antiprotons and its spread. Because of this we can reconstruct the beam characteristics from the data sample with high precision. The reconstructed momentum distribution of the incident antiprotons is determined by several effects: first, by a uniform smearing ($\sigma_{rms} \approx \pm 0.20$ MeV/c) due to the energy loss in a single target cell; second, by the reconstruction accuracy ($\sigma_{rms} \approx \pm 0.17$ MeV/c) of the analysis procedure; and third, by the momentum spread ($\sigma_{rms} \approx \pm 0.14$ MeV/c) in the extracted LEAR beam. The contribution due to energy straggling in the front beam-defining scintillators and within the single target cells can be estimated to be about 1% of the energy loss. From these numbers one obtains an overall spread of the reconstructed beam momentum of ± 0.30 MeV/c for a single target cell.

For the reconstructions of individual events an effective antiproton momentum is used that is chosen, based on a χ^2 criterion, to be one of the following three values: either the central momentum appropriate to the target cell in which the event took place; or one of two other momenta located at values ± 0.15 MeV/c around that central momentum. These momentum values fall within the overall spread in momentum of $\pm$ 0.30 MeV/c described above.

The threshold measurement was performed at two $\bar{p}$ momenta extracted from LEAR: 1449.1 MeV/c and 1440.7 MeV/c. The latter momentum setting was used also for measurements at two other momenta by inserting the degraders into the beam. Depending on the LEAR extraction momentum and the degrader settings, differential cross sections and polarizations were obtained for three ranges of the excess energy ε: $\varepsilon \leq 0.9$ MeV; $0.1 \leq \varepsilon \leq 1.2$ MeV; and $3.1 \leq \varepsilon \leq 4.2$ MeV.

To estimate the background contribution from the carbon present in the polyethylene targets T2-T5, the event sample produced by the carbon target cell T1 was analyzed. These events had clear signatures, allowing determinations of the carbon event cross sections and their subtraction from the CH_2 samples. The background contribution

which passed our event filter is about 6% compared with hyperon production on free protons in the energy range down to 0.3 MeV above threshold, and it increases to about 30% closer to the reaction threshold.

4. RESULTS

The differential cross section and polarization distributions are plotted in Figs. 2 and 3. The errors are statistical only, and include contributions due to the number of data events, the Monte Carlo simulation, and the overall normalization. The differential cross sections are the results of summing all events in all target cells at the corresponding LEAR beam and degrader settings. Table 1 lists the number of events obtained and the resulting total cross sections. The notations for the various beam settings used in Tables 1 and 2 are: (a) for an extraction momentum of 1440.7 MeV/c plus the 11mm degrader; (b) for 1440.7 MeV/c plus the 5 mm degrader; (c) for 1440.7 MeV/c; and (d) for 1449.1 MeV/c.

In Fig. 2 it can be seen that the $\bar{\Lambda}$ angular distributions are substantially forward-peaked even down to the reaction threshold. This anisotropy of the differential cross sections indicates that there are remarkably high contributions from partial waves of $l > 0$ even this close to threshold. The forward peaking rises rapidly with increasing $\bar{p}$ momentum, as observed in previous experiments [9,10].

The polarization of the Λ and $\bar{\Lambda}$ are evaluated from their asymmetric, self-analyzing, weak decays [9]. Since charge conjugation invariance in the creation process requires that $P(\Lambda) = P(\bar{\Lambda})$, we have averaged our Λ and $\bar{\Lambda}$ polarization data to produce the graph shown in Fig. 3. At excess energies $\varepsilon > 3.1$ MeV a clearly positive polarization structure can be seen. At the upper limit of the ε range, the full angular range corresponds to a squared four-momentum transfer of $-t' = -(t - t_{min}) \leq 0.17$ $(GeV/c)^2$. In previous measurements at higher energies [9-11], the polarization also shows positive values for small $-t'$ and changes sign at $-t' \approx 0.17$ $(GeV/c)^2$, independent of incident momentum. An explanation for this behavior has not yet been given.

Using the modular structure of the target, total cross sections are obtained for 16 different excess energies ε ranging from 0.85 MeV below the reaction threshold to 4.05 MeV above it. This energy range is given with respect to the center of the target. Fig. 4 displays the excitation function and Table 2 lists the cross section values for these 16 data points. The errors are statistical only as described above. Systematic errors are estimated by Monte Carlo studies to be less than 5%.

Assuming a constant transition matrix element, and neglecting dynamical and interference effects in the transition amplitudes, the energy dependence of the total cross section near threshold depends only on the angular momentum l viz. $\varepsilon^{l+1/2}$. However, it

is clear from Fig. 4 that the data cannot be described with either a $\varepsilon^{1/2}$ dependence (dotted line) or an $\varepsilon^{3/2}$ dependence (dashed line) alone. A fit to the data with a combination of s- and p-waves (solid line) indicates that a substantial p-wave admixture is required to describe the data even though they are so near to threshold. This confirms what is observed in the differential cross sections shown in Fig. 2.

Recently, attempts have been made to explain theoretically the threshold behavior of the reaction $\bar{p}p \rightarrow \bar{\Lambda}\Lambda$. From their calculations, Dalkarov *et al.* [2] conclude that there is a p-wave enhancement due to the existence of quasi-nuclear p-states near threshold in $\bar{N}N$ and $\bar{Y}Y$ systems. Kohno and Weise [3], using a kaon exchange model, deduce that there is s-wave suppression caused by initial- and final-state interactions. Both approaches lead to a rather strong p-wave contribution.

Figure 5 shows all existing experimental data for the reaction $\bar{\Lambda}\Lambda$ in the LEAR energy range [9-14]. Our data, together with the data of other experiments, show an increase of the total cross section from threshold to the maximum production strength of about 120 μb in the region of $p_{\bar{p}} = 2.0$ GeV/c.

ACKNOWLEDGEMENTS

The measurement presented here would not have been possible without the efforts of the staff of the CERN antiproton complex, and especially of the LEAR team, in preparing the high-quality $\bar{p}$ beams. We wish to thank them for their excellent and essential contribution to our experiment.

This work is based on a dissertation submitted by one of us (R. v. F.) to the University of Erlangen-Nürnberg in partial fulfillment of the requirements for the Ph.D. degree.

We gratefully acknowledge support from the Austrian Science Foundation, the German Federal Minister for Research and Technology (under contracts 0234 FR AI and 0234 ER A), the Swedish Natural Science Research Council, the United States Department of Energy, and the United States National Science Foundation.

REFERENCES

[1] F. Tabakin and R. A. Eisenstein, Phys. Rev. **C31** (1985) 371.

[2] O. D. Dalkarov, K. V. Protasov and I. S. Shapiro, P. N. Lebedev Inst., Moscow, preprint 37 (1988).

[3] M. Kohno and W. Weise, Nucl. Phys. **A479** (1988) 433c.

[4] R.´G. Timmermans, T. A. Rijken and J. J. de Swart, Nucl. Phys. **A479** (1988) 383c.

[5] M. A. Alberg, E. M. Henley and L. Wilets, Univ. Seattle preprint 40048-40 N7 (1988).

[6] M. Burkardt and M. Dillig, Phys. Rev. **C37** (1988) 1362.

[7] S. Furui and A. Faessler, Nuc. Phys. **A468** (1987) 669.

[8] P. Kroll and W. Schweiger, Nuc. Phys **A474** (1987) 608.

[9] P. D. Barnes *et al.*, Phys. Lett. **189B** (1987) 249.

[10] B. Jayet *et al.*, Nuovo Cimento **45A** (1978) 371.

[11] P. D. Barnes *et al.*, Phys. Lett. **199B** (1987) 147.

[12] J. W. Cruz, Ph.D. thesis, Rutgers State Univ. of New Jersey, 1983 (experiment BNL-E644).

[13] B. Y. Oh *et al.*, Nucl. Phys. **B51** (1973) 57.

[14] X. Xuong *et al.*, Phys. Rev. **128** (1962) 1849.

Table 1

Total cross sections of the reaction $\bar{p}p \rightarrow \bar{\Lambda}\Lambda$ averaged over all CH_2 target cells. The beam settings are described in the text. Also given are the number of good event candidates (those for which the reduced χ^2 is less than 5). The incident momentum value is for the center of the CH_2 target.

Beam Setting (see text)	Incident Momentum (MeV/c)	Excess Energy Range (MeV)	Number of Reconstructed Events	Total Cross Section (μb)
b	1435.6±1.6	<0.8	214	0.84 ± 0.20
c	1437.0± 1.6	0.1 - 1.2	374	1.44 ± 0.32
d	1445.4± 1.6	3.1 - 4.2	848	4.86 ± 0.42

Table 2

Total cross sections of the reaction $\bar{p}p \rightarrow \bar{\Lambda}\Lambda$ in the energy region between 0.85 MeV below the threshold and 4.05 MeV above it. The beam settings are described in the text. The resolution of the beam momentum is $\Delta p_{\bar{p}} = \pm 0.30$ MeV/c, corresponding to $\Delta\varepsilon = \pm 0.11$ MeV. Also given are the number of good event candidates (those for which the reduced χ^2 fell below 5). The incident momentum and excess energy are given with respect to the center of the target cell.

Beam Setting (see text)	Incident Momentum (MeV/c)	Excess Energy (MeV)	Number of Reconstructed Events	Total Cross Section (μb)
a	1432.65	-0.85	0	<0.09
a	1433.45	-0.57	0	<0.08
a	1434.25	-0.28	0	<0.07
b	1434.35	-0.24	5	0.07 ± 0.06
a	1435.05	-0.00	6	0.32 ± 0.16
b	1435.15	0.04	14	0.21 ± 0.08
c	1435.75	0.25	38	0.74 ± 0.14
b	1435.95	0.32	75	1.13 ± 0.14
c	1436.55	0.53	78	1.30 ± 0.16
b	1436.75	0.60	120	1.45 ± 0.15
c	1437.35	0.81	134	1.84 ± 0.17
c	1438.15	1.09	124	1.48 ± 0.15
d	1444.15	3.21	147	4.02 ± 0.37
d	1444.95	3.49	174	4.26 ± 0.36
d	1445.75	3.77	246	5.14 ± 0.36
d	1446.55	4.05	281	5.34 ± 0.35

Figure Captions

Fig. 1 Scale drawing of the target for experiment PS185. The incoming antiproton beam is defined by a coincidence between S1A and S1B. The first target T1 is pure carbon, while targets T2-T5 are polyethylene (CH_2). The veto and beam-tagging counters for each cell are labelled by S2 and S3.

Fig. 2 Differential cross sections for the reaction $\bar{p}p \rightarrow \bar{\Lambda}\Lambda$ from three independent measurements at incident $\bar{p}$ momenta in the intervals: $p_p \leq 1437.2$ MeV/c; $1435.2 \leq p_p \leq 1438.6$ MeV/c; and $1443.7 \leq p_p \leq 1447.0$ MeV/c. The excess energy ranges are indicated.

Fig. 3 Combined polarization for $\bar{\Lambda}$ and Λ obtained for ε regions as shown in Fig. 2. The scale of the reduced squared four-momentum transfer $-t' = -(t_{min} - t)$ is indicated; it corresponds to the upper limit of the ε region.

Fig. 4 Total cross sections for the reaction $\bar{p}p \rightarrow \bar{\Lambda}\Lambda$ in the threshold region. The data are fitted (solid line) with the function $\sigma_{tot} = b_0\varepsilon^{1/2} + b_1\varepsilon^{3/2}$. The phenomenological parameters are given by $b_0 = 1.51$ μb/MeV$^{1/2}$ and $b_1 = 0.26$ μb/MeV$^{3/2}$. The dotted line represents a pure s-wave (b_0 as given, b_1=0); the dashed line a pure p-wave ($b_0 = 0$, b_1 as given).

Fig. 5 Compilation of available $\bar{p}p \rightarrow \bar{\Lambda}\Lambda$ cross-section data in the LEAR energy range. The data are taken from this experiment and from refs. [9-14].

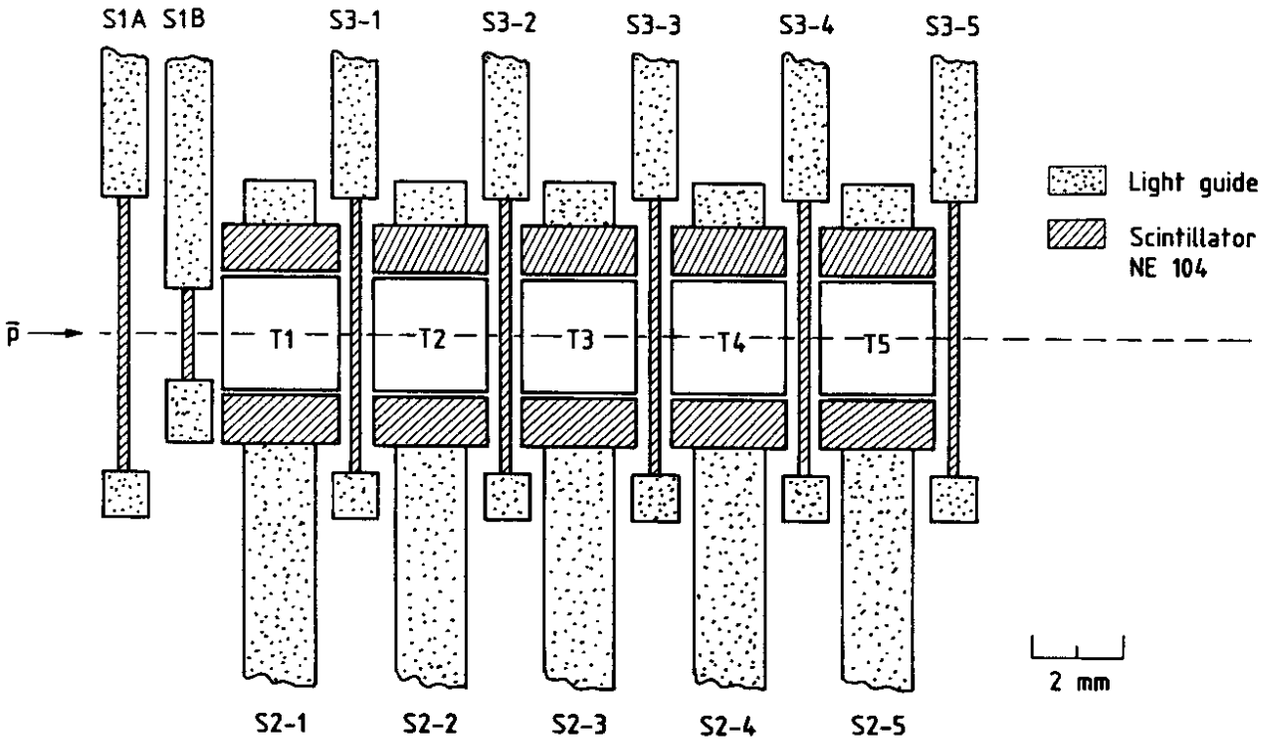
S1A
S1B
S3-1
S3-2
S3-3
S3-4
S3-5
p̄
T1
T2
T3
T4
T5
Light guide
Scintillator
NE 104
2 mm
S2-1
S2-2
S2-3
S2-4
S2-5

Figure 1

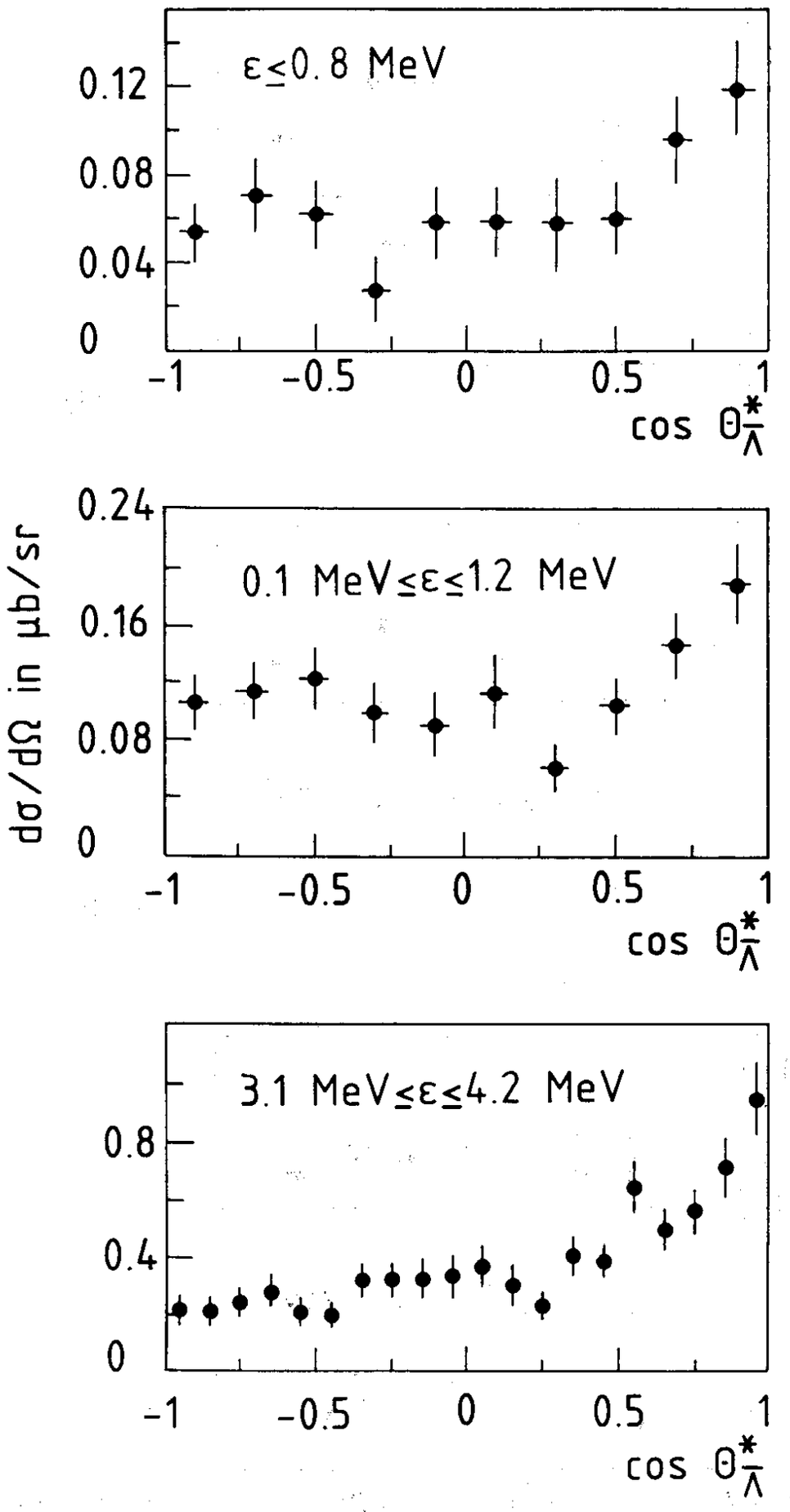
ε≤0.8 MeV
0.12
0.08
0.04
0
-1
-0.5
0
0.5
1
cos Θ*Λ
dσ/dΩ in μb/sr
0.1 MeV≤ε≤1.2 MeV
0.24
0.16
0.08
0
3.1 MeV≤ε≤4.2 MeV
0.8
0.4

Figure 2

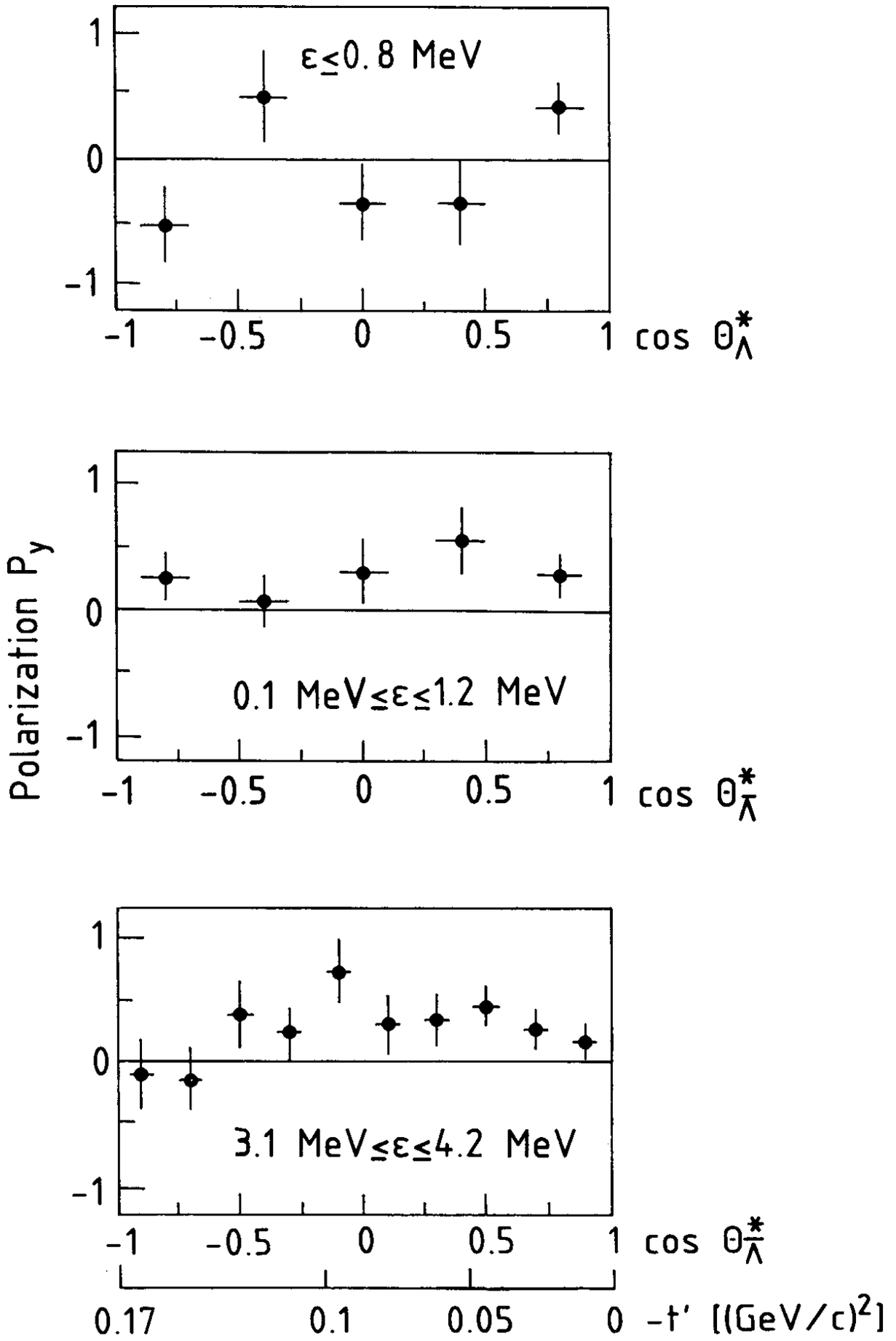
ε≤0.8 MeV
0.1 MeV≤ε≤1.2 MeV
3.1 MeV≤ε≤4.2 MeV
Polarization P_y
1
0
-1
-1
-0.5
0
0.5
1
cos Θ^*_Λ
0.17
0.1
0.05
0
-t' [(GeV/c)^2]

Figure 3

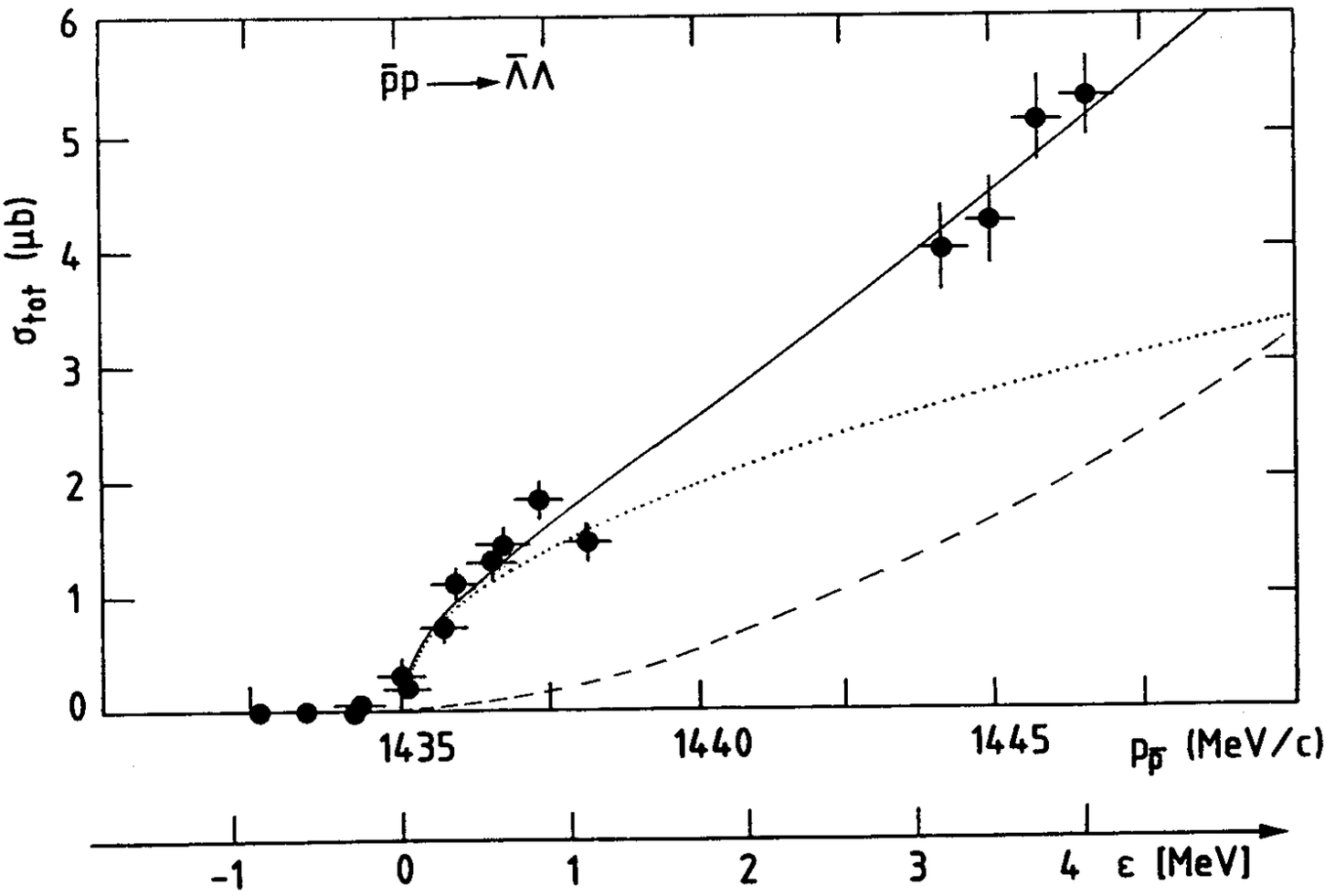
$\bar{p}p \longrightarrow \bar{\Lambda}\Lambda$
σ_{tot} (μb)
0
1
2
3
4
5
6
1435
1440
1445
$p_{\bar{p}}$ (MeV/c)
-1
0
1
2
3
4
ε [MeV]

Figure 4

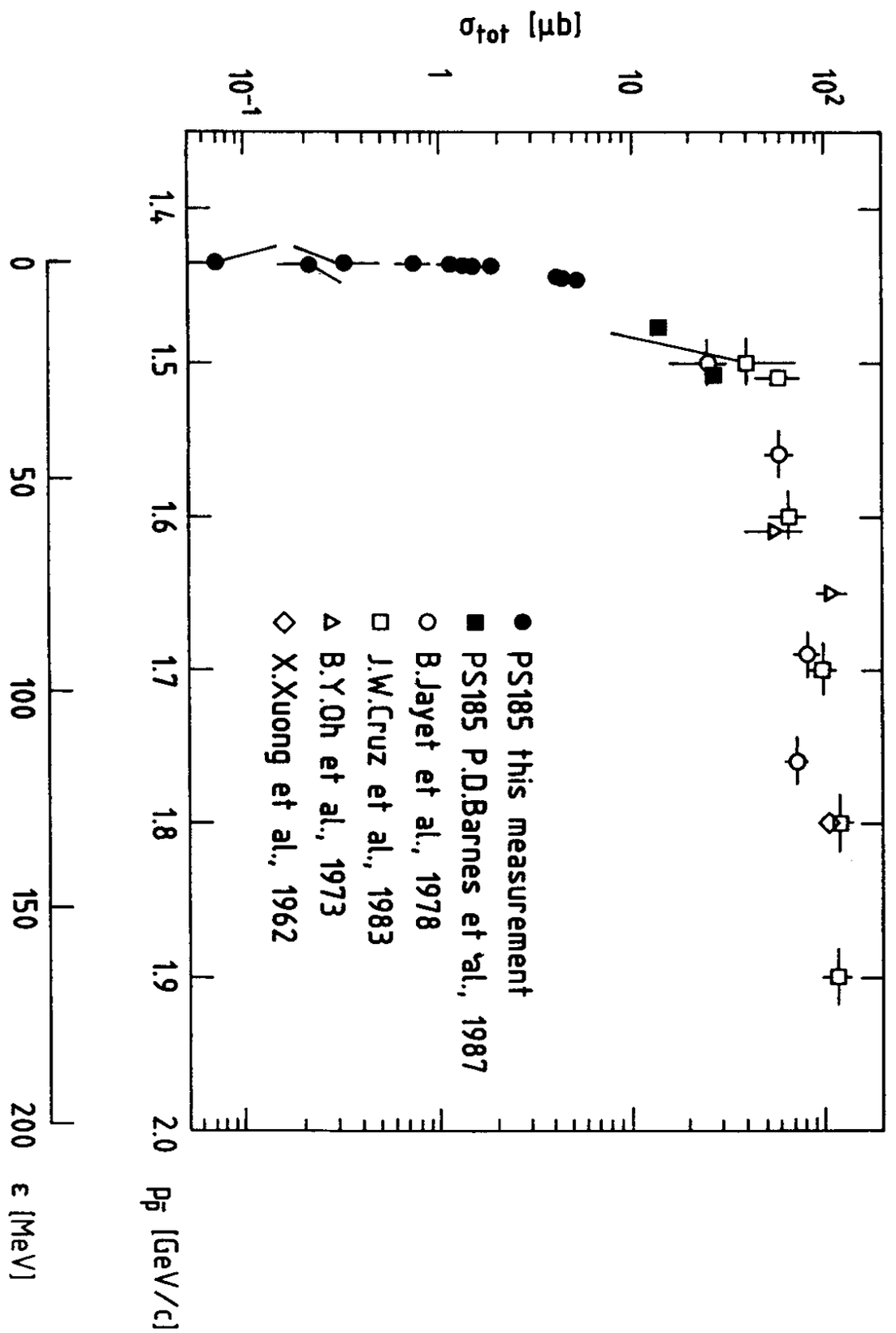
σ_{tot} [μb]
10^2
10
1
10^{-1}
● PS185 this measurement
■ PS185 P.D.Barnes et al., 1987
○ B.Jayet et al., 1978
□ J.W.Cruz et al., 1983
△ B.Y.Oh et al., 1973
◇ X.Xuong et al., 1962
1.4
1.5
1.6
1.7
1.8
1.9
2.0
$p_{\bar{p}}$ [GeV/c]
0
50
100
150
200
ε [MeV]

Figure 5